十二指腸晶片：
臨床前藥代動力學研究利器

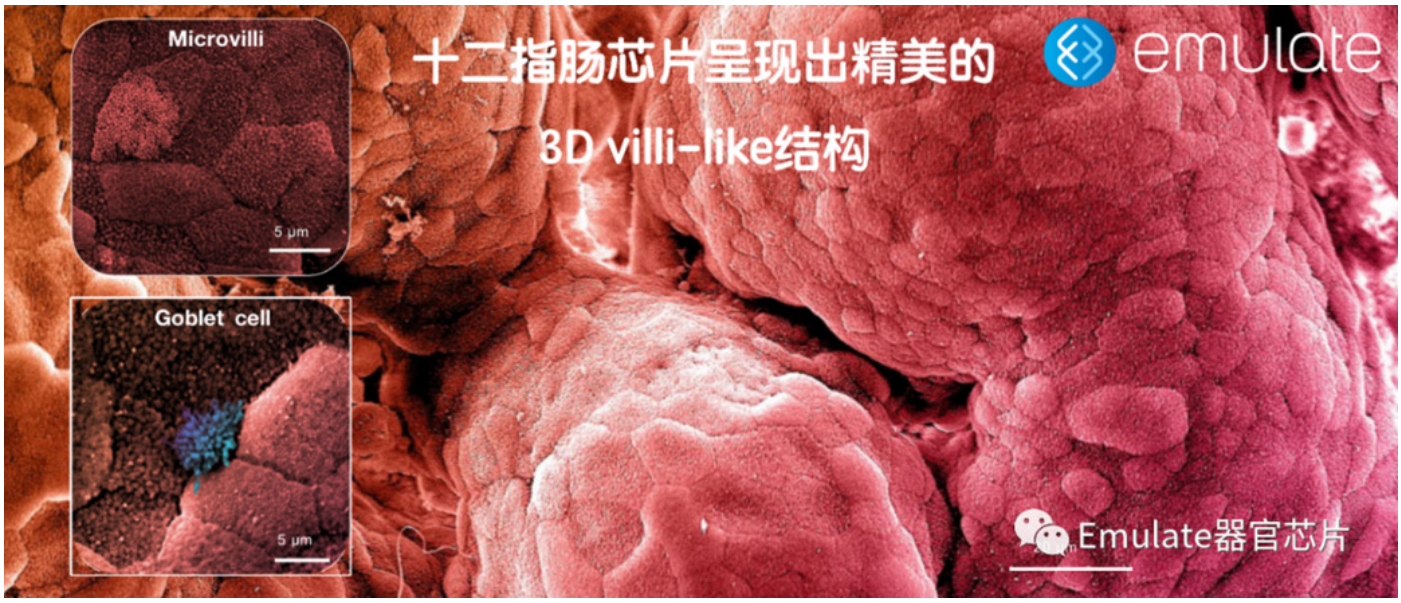

準確評估藥代動力學（PK）是現代藥物開發中重要工作。藥物的複雜特性（溶解度、滲透性）、腸道的生理學（轉運時間、血流）和病人的表型（包括年齡、性別、藥物代謝酶的多態性、疾病狀態）差異等，導致體外準確預測藥物在腸道中的口服生物利用度和準確評估藥代動力學挑戰巨大。

摘要

動物模型局限性

受限於藥物代謝酶和細胞轉運體的物種差異，以及調節轉錄啟動的機制不同，動物模型的資料難以推導到臨床。例如，在小鼠中，參與藥物代謝的主要基因家族中有 34 個細胞色素 P450（CYP），即 CYP1A、CYP2C、CYP2D 和 CYP3A 基因簇，而在人類中只有 8 個。有趣的是，三種人類酶，CYP2C9、CYP2D6 和 CYP3A4，占所有反應的 75%，其中 CYP3A4 是唯一最重要的人類 CYP450，占人類第一階段藥物代謝的 45%。此外，許多主要的人類 CYP450 酶和藥物轉運體（決定藥物暴露的水準和變化）的表達水準受多種轉錄因數的控制，這些重要的因素均表現出明顯的物種差異。加上腸道和肝臟中藥物代謝酶和藥物轉運體之間複雜的相互作用，以及底物和抑制劑特異性的重疊，使得在藥物開發的臨床前階段很難預測人類藥代動力學。

2D 細胞局限性

目前已有一些臨床前體外非動物模型被應用於潛在候選藥物在人體中的吸收、分佈、代謝和排泄（ADME）的描述和預測。其中，Caco-2 單層培養在 transwell 嵌件上，作為人類小腸的體外代表，它是整個製藥業使用最多的模型之一。然而，缺乏體內相關的三維（3D）細胞結構，缺乏適當的細胞群比例，藥物轉運體和藥物代謝酶的表達譜改變（尤其是 CYP450 酶家族），以及異常的 CYP450 誘導反應，對使用這些傳統模型來預測人類在臨床上的反應提出了挑戰。

3D 類器官球局限性

隨著3D腸道類器官的技術的發展，替代傳統單層細胞培養的方法已逐漸顯現。使用3D類器官，可應用多種不同的研究方向，包括器官發育、疾病建模和再生醫學。然而，3D類器官在藥代動力學研究仍然非常有限。主要局限性為類器官的3D球體緻密導致其球體內部細胞的滲透性降低，甚至很多內部細胞已經缺氧而死亡，導致評估整個球體的滲透性或藥物吸收性能大打折扣。此外，傳統培養3D類器官球是非常耗時耗力的過程，並且球的外表面細胞通常被非常厚的基質膠（如Matrigel）所包埋，可能會進一步限制藥物的滲透。同時，體外無序培養而成的器官結構，其大小、形狀和活力方面的異質性，造成難以統一和標準化，也會阻礙藥代動力學的研究。

Emulate 器官晶片亮點

本研究中，Emulate 的研究人員開發了原代十二指腸器官晶片模型，類比腸道組織結構和功能，用於研究藥代動力學和藥物相互作用。十二指腸腸道晶片顯示了高度成熟，且與生理相關度更高的極化上皮細胞結構，並呈現出與體內類似的屏障功能。轉錄組學分析表明，相比于單層細胞和3D類器官體系，器官晶片的基因表達譜與體內更為接近，尤其是針對於藥物轉運和代謝相關的分子。與單層細胞的器官晶片培養體系相比，Emulate十二指腸器官晶片模型顯示出更好的CYP3A4表達和誘導能力。重要的是，將 Emulate十二指腸腸道晶片暴露於CYP450誘導劑，如利福平和骨化三醇，導致 CYP3A4 mRNA、蛋白質水準和藥物代謝活性明顯增加。我們的結果表明，3D 類器官衍生的十二指腸細胞可以與Emulate器官晶片技術相結合，為CYP450介導的代謝、藥物轉運體的活性和藥物相互作用風險的臨床前評估提供一個強大平臺。Emulate標準化的十二指腸器官晶片模型的建立可以更好地預測人類藥代動力學和藥物相互作用風險。

主要亮點

1. 受限於藥物代謝酶和細胞轉運體的物種差異，以及調節轉錄啟動的機制不同，動物模型的藥代動力學資料難以推導到臨床。
2. 傳統3D腸道類器官球體內部緻密，並且周身包圍於基質膠，藥物難以滲透。加上靜態體系中的無序培養，不同球體在大小、形狀、結構上差異巨大，難以標準和統一化，導致研究藥代動力學和藥物相互作用困難巨大。
3. Emulate的研究人員開發了原代十二指腸器官晶片模型，類比腸道組織結構和功能，用於研究藥代動力學和藥物相互作用。並且作為標準化的商品，可供用戶迅速在自己實驗室建立模型。

研究詳情

eLIFE elifesciences.org

RESEARCH ARTICLE

Duodenum Intestine-Chip for preclinical drug assessment in a human relevant model

Magdalena Kasendra[1†*], Raymond Luc[1†], Jianyi Yin[2], Dimitris V Manatakis[1], Gauri Kulkarni[1], Carolina Lucchesi[1], Josiah Sliz[1], Athanasia Apostolou[1,3], Laxmi Sunuwar[2], Jenifer Obrigewitch[1], Kyung-Jin Jang[1], Geraldine A Hamilton[1], Mark Donowitz[2], Katia Karalis[1]

[1]Emulate Inc, Boston, United States; [2]Department of Medicine, Division of Gastroenterology, Johns Hopkins University School of Medicine, Baltimore, United States; [3]Graduate Program, Department of Medicine, National and Kapodistrian University of Athens, Athens, Greece

Abstract Induction of intestinal drug metabolizing enzymes can complicate the development of new drugs, owing to the potential to cause drug-drug interactions (DDIs) leading to changes in pharmacokinetics, safety and efficacy. The development of a human-relevant model of the adult intestine that accurately predicts CYP450 induction could help address this challenge as species differences preclude extrapolation from animals. Here, we combined organoids and Organs-on-Chips technology to create a human Duodenum Intestine-Chip that emulates intestinal tissue architecture and functions, that are relevant for the study of drug transport, metabolism, and DDI. Duodenum Intestine-Chip demonstrates the polarized cell architecture, intestinal barrier function, presence of specialized cell subpopulations, and *in vivo* relevant expression, localization, and function of major intestinal drug transporters. Notably, in comparison to Caco-2, it displays improved CYP3A4 expression and induction capability. This model could enable improved *in vitro* to *in vivo* extrapolation for better predictions of human pharmacokinetics and risk of DDIs.

***For correspondence:** magdalena.kasendra@gmail.com

[†]These authors contributed equally to this work

Competing interest: See page 19

Funding: See page 19

Received: 12 July 2019
Accepted: 18 December 2019
Published: 14 January 2020

Reviewing editor: Milica Radisic, University of Toronto, Canada

© Copyright Kasendra et al. This article is distributed under the terms of the Creative Commons Attribution License, which permits unrestricted use and redistribution provided that the original author and source are credited.

Introduction

Low bioavailability and pharmacokinetics caused by drug-drug interactions of orally administered drugs represents a significant challenge in the modern drug development. High affinity of certain drugs for cellular transporters combined with the extensive activity of metabolic enzymes present in the human intestine are the main factors limiting drug bioavailability (***Dietrich, 2003***; ***Thummel, 2007***; ***Shugarts and Benet, 2009***; ***Peters et al., 2016***). After decades of research, the hepatic drug clearance is well-understood and relatively well predicted by pre-clinical models, while the accurate prediction of the first-pass extraction of xenobiotics in human intestinal epithelium still remains elusive. This is due to a number of confounding factors that affect oral drug absorption including the properties of the compound (solubility, permeability), physiology of the intestinal tract (transit time, blood flow), and patient phenotype (including age, gender, polymorphism in drug metabolizing enzymes, disease states) (***Pang, 2003***). Species differences in the isoforms, regional abundances, differences in substrate specificity of drug metabolism enzymes (***Martignoni et al., 2006***; ***Paine et al., 2006***; ***Komura and Iwaki, 2011***) and transporters (***Tucker et al., 2012***; ***Gröer et al., 2013***), and mechanism regulating transcriptional activation (***LeCluyse, 2001***; ***Mackowiak et al., 2018***), precludes accurate extrapolation of the data from animal models to the clinic. In mice, for example, there are 34 cytochrome P450 (CYPs) in the major gene families involved in drug metabolism, that is the *CYP1A*, *CYP2C*, *CYP2D*, and *CYP3A* gene clusters, while in humans,

Emulate器官芯片

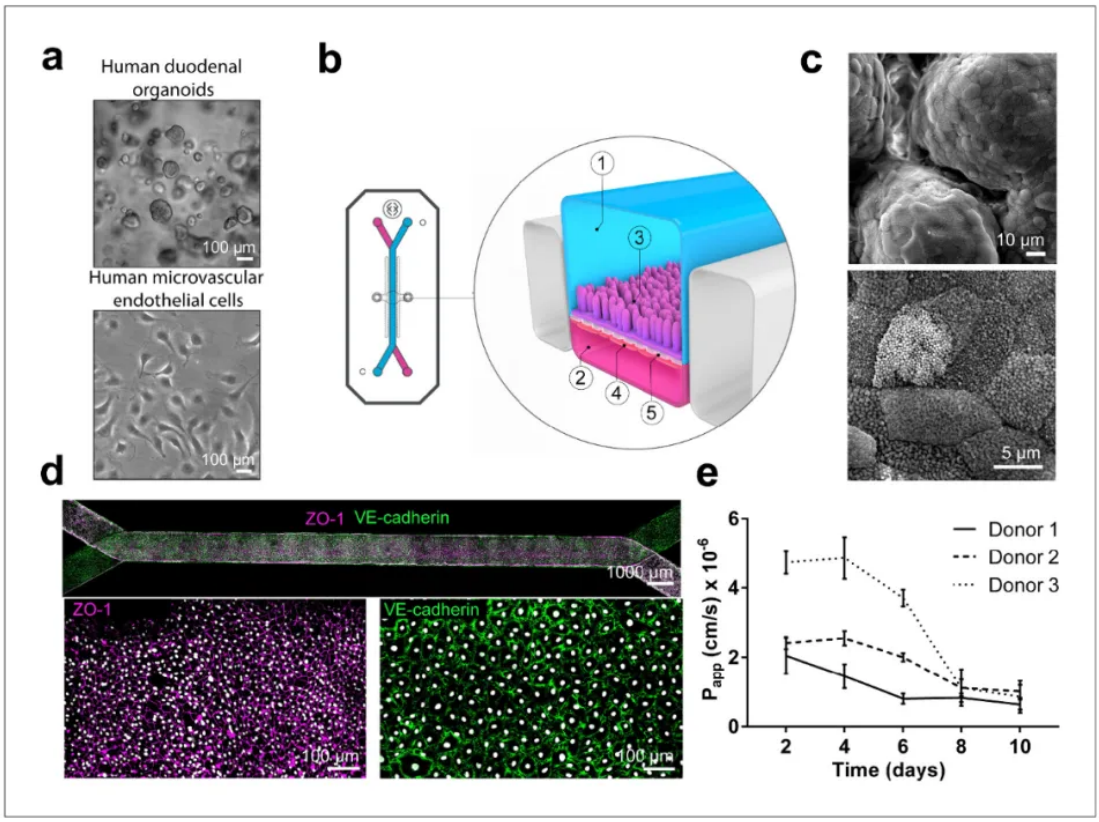

Figure 1. Duodenum Intestine-Chip: a microengineered model of the human duodenum. (**a**) Brightfield images of human duodenal organoids (top) and human microvascular endothelial cells (bottom) acquired before their seeding into epithelial and endothelial channels of the chip, respectively. (**b**) Schematic representation of Duodenum Intestine-Chip, including its top view (left) and vertical section (right) showing: the epithelial (1; blue) and vascular (2; pink) cell culture microchannels populated by intestinal epithelial cells (3) and endothelial cells (4), respectively, and separated by a flexible, porous, ECM-coated PDMS membrane (5). (**c**) Scanning electron micrograph showing complex intestinal epithelial tissue architecture achieved by duodenal epithelium grown for 8 days on the chip (top) in the presence of constant flow of media (30 µl/hr) and cyclic membrane deformations (10% strain, 0.2 Hz). High magnification of the apical epithelial cell surface with densely packed intestinal microvilli (bottom). See Figure 1-figure supplement demonstrating the effect of mechanical forces on the cytoarchitecture of epithelial cells and the formation of intestinal microvilli (**d**) Composite tile scan fluorescence image 8 days post-seeding (top) showing a fully confluent monolayer of organoid-derived intestinal epithelial cells (magenta, ZO-1 staining) lining the lumen of Duodenum Intestine-Chip and interfacing with microvascular endothelium (green, VE-cadherin staining) seeded in the adjacent vascular channel. Higher magnification views of epithelial tight junctions (bottom left) stained against ZO-1 (magenta) and endothelial adherence junctions visualized by VE-cadherin (bottom right) staining. Cells nuclei are shown in gray. Scale bars, 1000 µm (top), 100 µm (bottom) (**e**) Apparent permeability values of Duodenum Intestine-Chips cultured in the presence of flow and stretch (30 µl/hr; 10% strain, 0.2 Hz) for up to 10 days. Papp values were calculated from the diffusion of 3 kDa Dextran from the luminal to the vascular channel. Data represent three independent experiments performed with three different chips/donor, total of three donors; Error bars indicate s.e.m.

The online version of this article includes the following figure supplement(s) for figur

Emulate器官芯片

Figure supplement 1. Flow-induced increase in primary intestinal epithelial cells height and microvilli formation.

specific markers in the Duodenum Intestine-Chip established from the cells of three different donors. Specific genes included: alkaline phosphatase (*ALPI*) for absorptive enterocytes, mucin 2 (*MUC2*) for goblet cells, chromogranin A (*CHGA*) for enteroendocrine cells, and lysozyme (*LYZ*) for Paneth cells. In addition, we compared the expression levels of these genes in a chip and in freshly isolated adult duodenal tissue (Duodenum). As shown in ***Figure 2A***, expression of most of the markers tested, with the exception of lysozyme, increased over time in culture. Notably, on day 8 of chip culture the mRNA expression of alkaline phosphatase and mucin two reached levels similar to

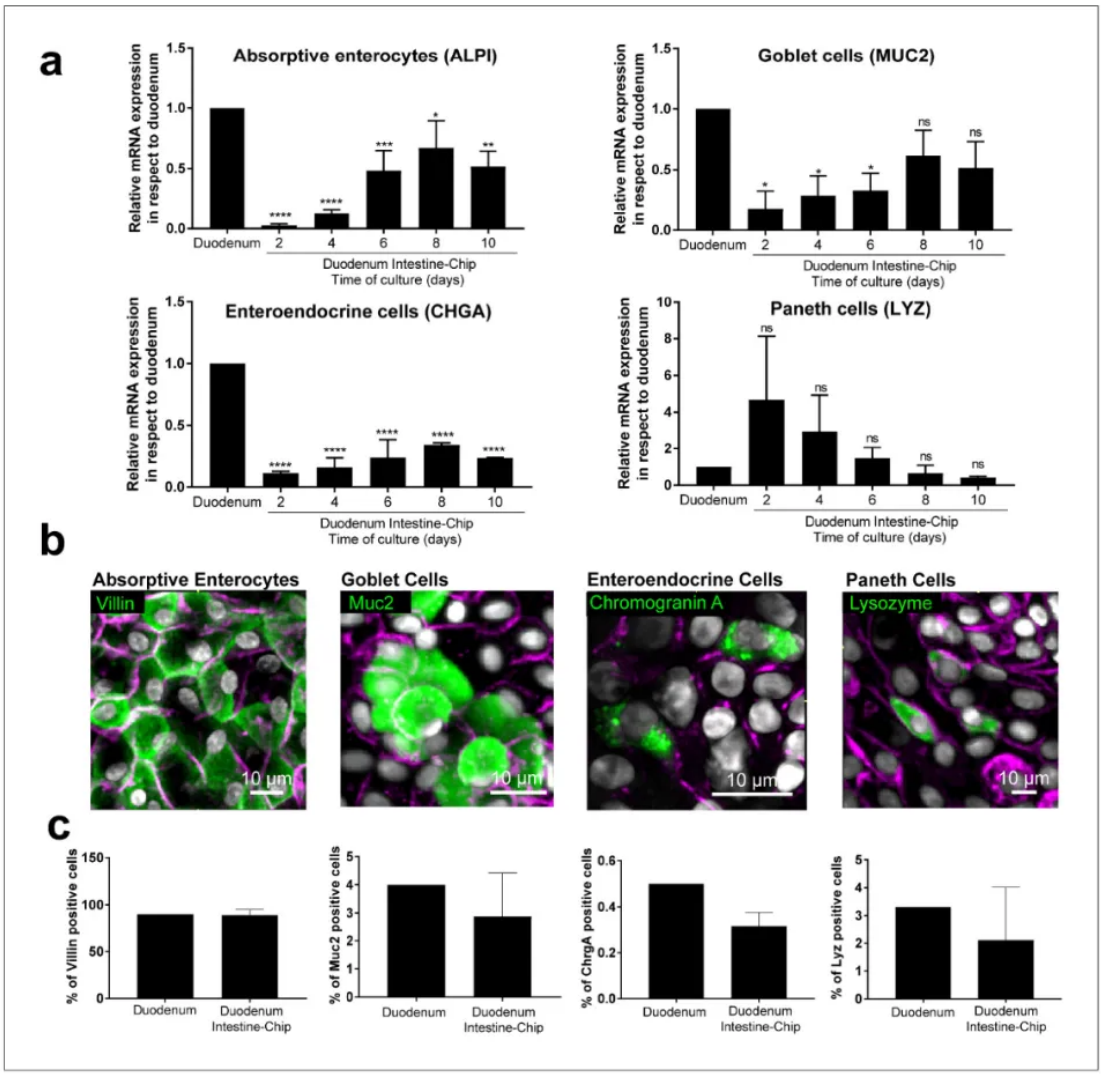

Figure 2. Duodenum Intestine-Chip emulates multi-lineage differentiation of native human intestine. (**a**) Comparison of the relative gene expression levels of markers specific for differentiated intestinal cell types, including mucin 2 (*MUC2*) for goblet cells, alkaline phosphatase (*ALPI*) for absorptive enterocytes, chromogranin A (*CHGA*) for enteroendocrine cells, lysozyme (*LYZ*) for Paneth cells in Duodenum Intestine-Chip and RNA isolated directly from the duodenal tissue (Duodenum). Expression of these genes at different time points (days 2, 4, 6, 8, 10) of Duodenum Intestine-Chip culture is shown. In each graph, values represent average gene expression ± s.e.m (error bars) from three independent experiments, each using different donors of biopsy-derived organoids and at least three different chips per time point. Values are shown relative to duodenal tissue expressed as 1. EPCAM expression is used as normalizing control. One-way ANOVA, ****p<0.0001, ***p<0.001, **p<0.01, *p<0.05, ns p>0.05. (**b**) Representative confocal fluorescent micrographs demonstrating the presence of all major intestinal cell types (green) in Duodenum Intestine-Chip at day 8 of fluidic culture, including goblet cells stained with anti-mucin-2; enteroendocrine cells visualized with anti-chromogranin A, absorptive enterocytes stained with anti-villin and Paneth cells labeled with anti-lysozyme. Cell-cell borders were stained with anti-E-cadherin and are shown in magenta. Cells nuclei are shown in gray. Scale bar, 10 µm. (**c**) Quantification of the different intestinal epithelial cell types present in Duodenum Intestine-Chip at day eight and identified by immunostaining, as described in (**b**). Cell ratios are based on 10 different fields of view (10 FOV) counted in three individual chips (each from a different donor) per staining. DAPI staining was used to evaluate the total cell number. Duodenum values, represent cell ratios observed in the histological sections and are based on the literature (***Karam,***

Emulate器官芯片

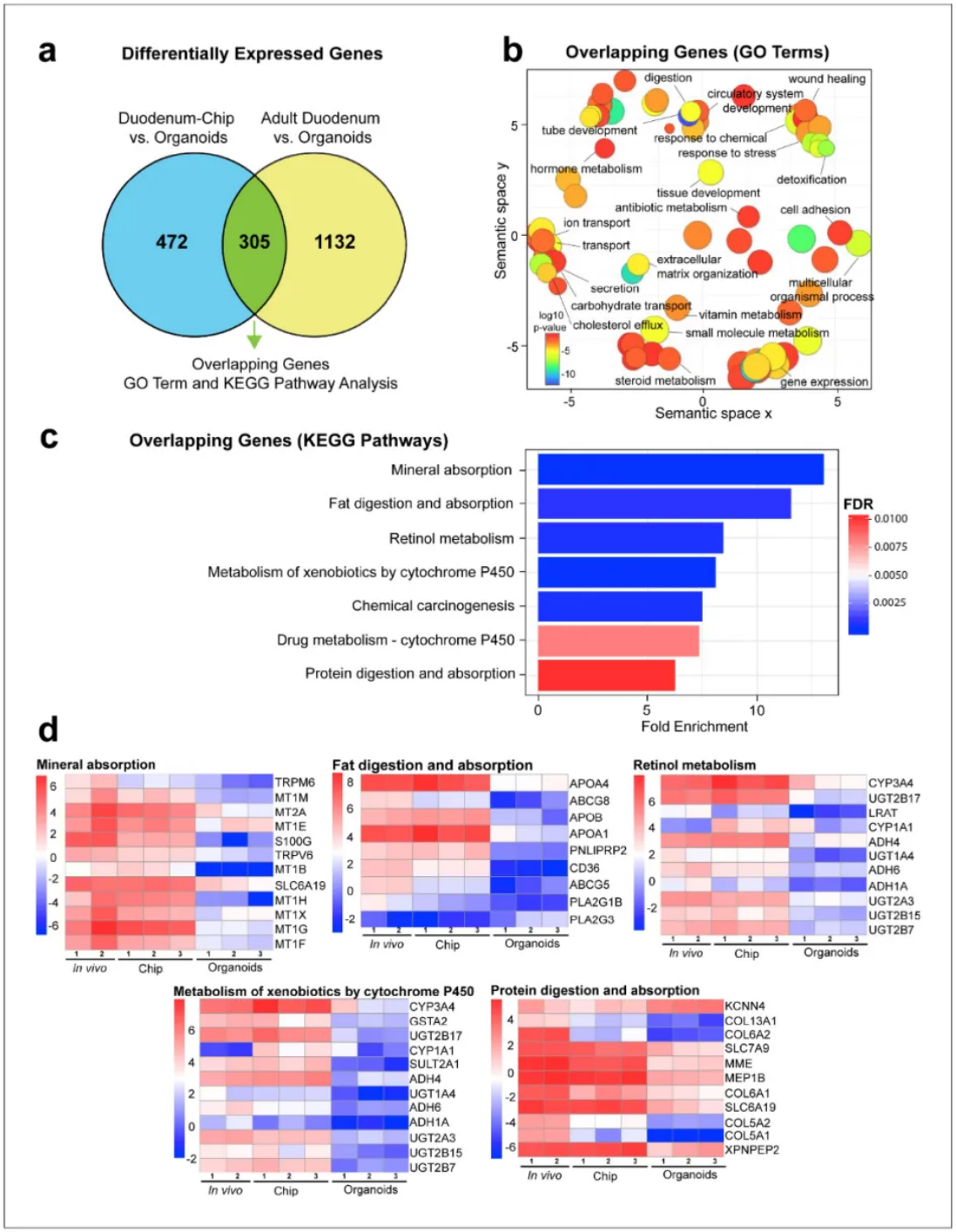

Figure 3. Duodenum Intestine-Chip exhibits higher transcriptomic similarity to adult duodenal tissue than organoid culture. (**a**) Differential gene expression analysis was carried out to identify genes that are up- or down-regulated in Duodenum Intestine-Chip compared to organoids (blue circle) (***Figure 3—source data 1***) and adult duodenum compared to organoids (yellow circle) (***Figure 3—source data 2***). The gene lists were then compared to determine how many genes overlap between those two comparisons (***Figure 3—source data 3***), and the results are shown as a Venn diagram. 305 genes were identified as common and responsible for the closer resemblance of Duodenum Intestine-Chip to human adult duodenum than organoids from which chips were derived. Sample sizes were as follows: Duodenum Intestine-Chip, n = 3 (independent donors); Organoids, n = 3 (independent donors); Adult duodenum, n = 2 (independent biological specimens). Intestinal crypts derived from the same three independent donors were used for the establishment of Duodenum Intestine-Chip and organoid cultures. Both chips and organoids were cultured in parallel, in the presence of expansion media for 6 days, followed by 2 days of differentiation media. Experiment was terminated and samples were processed for analyses 8 days post-seeding. (**b**) The list of overlapping genes was subjected to GO analysis to identify enriched biological processes (GO terms) (***Figure 3—source data 4***). The results are shown as REVIGO scatterplots in which similar GO terms are grouped in arbitrary two-dimensional space based on semantic similarity. Each circle corresponds to a specific GO term and circle sizes are proportional to the number of genes included in each of the enriched GO

Figure 3 continued on next page

Emulate器官芯片

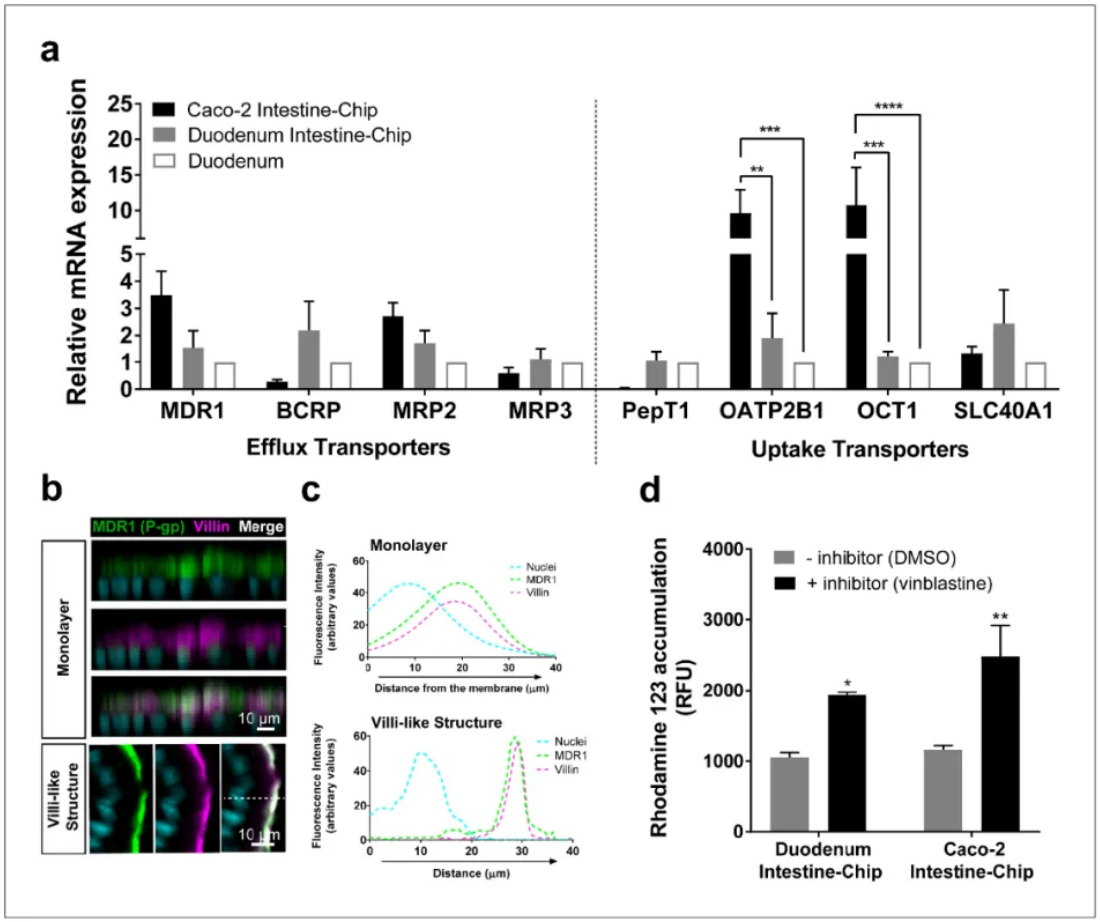

Figure 4. Duodenum Intestine-Chip shows the presence of major intestinal drug transporters and correct localization and function of efflux pump MDR1 (P–gp). (**a**) Comparison of the relative average gene expression levels of drug efflux (MDR1, BCRP, MRP2, MRP3) and uptake (PEPT1, OATP2B1, OCT1, SLC40A1) transporters in Caco-2 Intestine-Chip, Duodenum Intestine-Chip, both assessed on day 8 of culture, and RNA isolated directly from the duodenal tissue (Duodenum). The results show that Duodenum Intestine-Chip expresses drug transport proteins at the levels close to human duodenal tissue. Note, the expression of OATP2B1 and OCT1 in Caco-2 Intestine-Chip were significantly higher than in human duodenum while the difference between Duodenum Intestine-Chip and adult duodenum is not significant. Each value represents average gene expression ± s.e.m (error bars) from three independent experiments, each involving Duodenum Intestine-Chip established from a tissue of three different donors (three chips/donor), RNA tissue from three independent biological specimens, and Caco-2 Intestine-Chip (three chips). Values are shown relative to the duodenal tissue expressed as 1, two-way ANOVA, ****p<0.0001, ***p<0.001, **p<0.01. EPCAM expression was used as normalizing control. (**b**) Representative confocal immunofluorescence micrographs showing apical localization of the efflux transporter MDR1 (green) and the cell surface marker villin (magenta) in a vertical cross section of monolayer (top) formed in Duodenum Intestine-Chip at day 4 and later formed villi-like structure (bottom) at day 8. Cell nuclei are visualized in cyan. Scale bar, 10 µm. (**c**) Line plots corresponding to confocal images in (b) showing the distribution of fluorescent intensities for three different channels: MDR1 (green), villin (magenta) and nuclei (cyan) along the basal–apical axis of enterocytes forming a monolayer or villi-like structures in Duodenum Intestine-Chip. The fluorescent intensity was analyzed in 3D reconstructed confocal images of Duodenum Intestine-Chip and plotted as average across 20 different z-stacks. Distribution of MDR1 and villin shows significant overlap. See also ***Figure 4—figure supplement 1*** showing luminal localization of additional efflux (BCRP) and uptake (PEPT1) transporters in Duodenum Intestine-Chip. (**d**) Activity of efflux pump proteins in Caco-2 and Duodenum Intestine-Chip. The intracellular accumulation of the fluorescent substrate of MDR1 - Rhodamine 123 is significantly increased in response to the MDR1 inhibitor vinblastine (black bars) in comparison to vehicle (DMSO) control (gray bars) in Caco2 and Duodenum Intestine-Chip. Data were represented as mean ± s.e.m (error bars) of at least three independent experiments involving chips generated from organoids of three individual donors or Caco-2 cells, all assessed 8 days post-seeding. Two-way ANOVA, **p<0.01, *p<0.05.

The online version of this article includes the following figure supplement(s) for figure 4:

Figure supplement 1. Luminal localization of efflux (BCRP) and uptake (PEPT1) transporters in Duodenum Intestine-Chip.

Emulate器官芯片

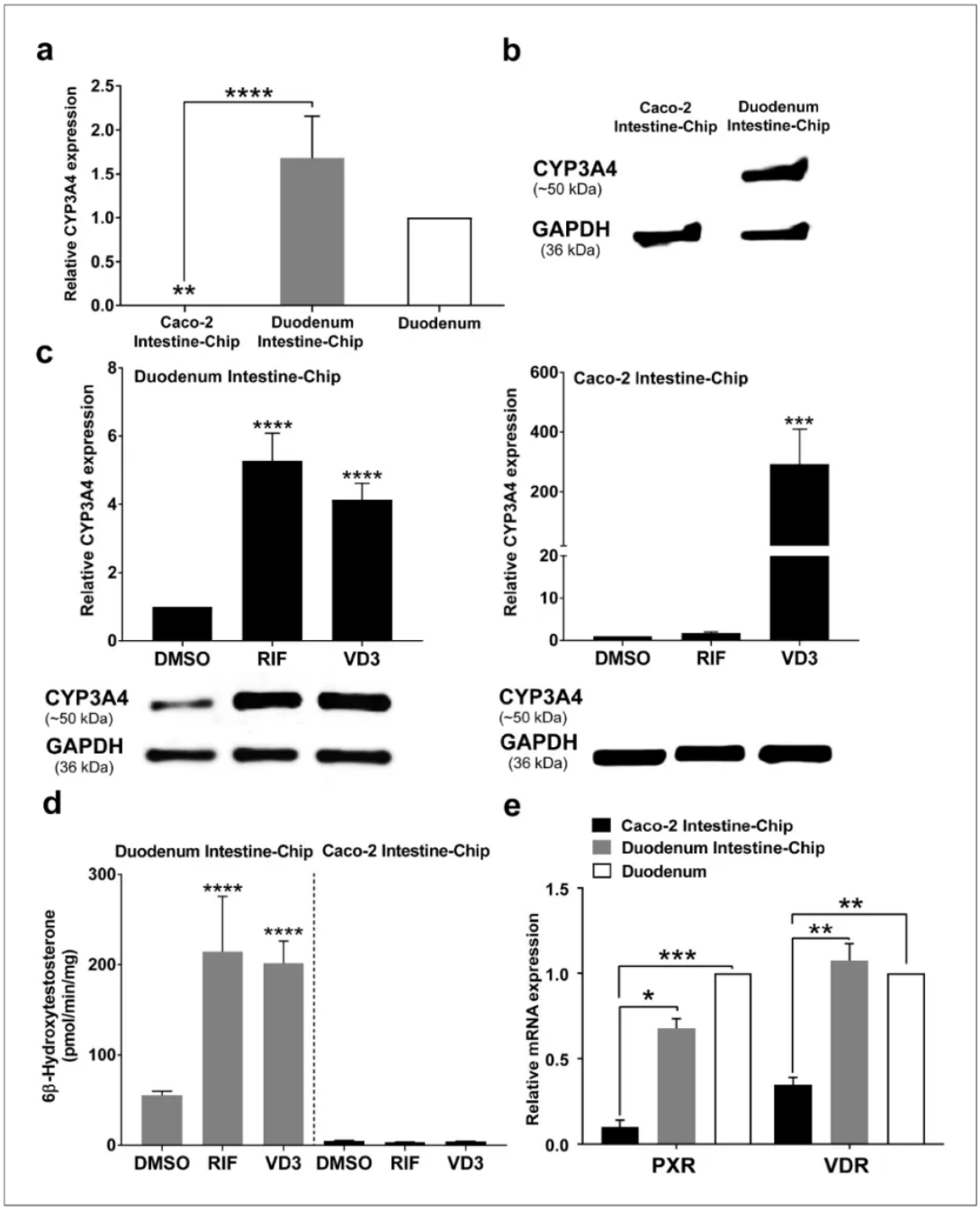

Figure 5. CYP3A4 expression levels and induction in Duodenum Intestine-Chip and Caco-2 Intestine-Chip. (**a**) Average gene expression levels of CYP3A4 ± s.e.m (error bars) in Caco-2 Intestine-Chip, Duodenum Intestine-Chip assessed at day 8 of their culture and human duodenum (three independent biological specimens). All values are shown relative to the adult duodenal tissue expressed as 1, one-way ANOVA, ****p<0.0001, **p<0.01. EPCAM expression was used as normalizing control. (**b**) Protein analysis of CYP3A4 in Caco-2 and Duodenum Intestine-Chip assessed at day eight using western blot. (**c**) The CYP3A4 induction in Duodenum Intestine-Chip and Caco-2 Intestine-Chip treated at day 6 with solvent (DMSO), 20 µM rifampicin (RIF) or 100 nM 1,25-dihidroxyvitamin D3 (VD3) for 48 hr. The gene expression levels (top) of CYP3A4 were examined by real-time PCR analysis at day 8. On the y-axis, the gene expression levels in the DMSO-treated chips were taken as 1.0. All data are represented as means ± s.e.m. Two-way ANOVA, ****p<0.0001 (compared with DMSO-treated cells). The corresponding CYP3A4 protein expression levels (bottom) were measured at day 8 by western blotting analysis. (**d**) CYP3A4 enzyme activity was determined by monitoring the formation of 6β-hydroxytestosterone in the medium of Duodenum Intestine-Chip and Caco-2 Intestine-Chip, as measured by LC-MS. For induction studies, 20 µM RIF or 100 nM VD3 was added 48 hr before measurement. Data are expressed as mean ± s.e.m of three independent experiments each involving Duodenum Intestine-Chip established from organoid-derived cells of a different donor and Caco-2 Intestine-Chip. At least three different chips were used per condition. Two-way ANOVA, ****p<0.0001 (**e**) Gene expression analysis of the receptors PXR and VDR in Duodenum Intestine-Chip and Caco-2 Intestine-Chip examined at day 8 by real-time PCR analysis and compared to their expression in adult duodenal tissue

Figure 5 continued on next page

Emulate器官芯片

關於 Emulate

器官晶片的開創性工作是由哈佛大學 WYSS 研究所的系主任 Donald E. Ingber 院士團隊完成的，其在Science發表了器官晶片領域具有里程碑意義的第一個成功的模型：肺晶片。之後，Donald E. Ingber 院士作為共同創始人，成立了 Emulate 公司，將器官晶片技術商業化運行，與更廣泛的生命科學界同仁分享這一精妙的器官晶片技術。自成立以來，我們致力於開發高度類比人體生理特徵的器官晶片技術和不同類型的創新應用，以全面瞭解疾病發生規律和幫助評估藥物的真實反應，改善人類健康。目前，Emulate 提供經過驗證的肝、腎、十二指腸、結腸、肺、腦等器官晶片解決方案的同時支援客戶定制化的研究需求，是全球市場佔有率領先的器官晶片品牌。全球系統裝機量超過 400 台，已經被全球排名前 20 的藥企全部合作引入，採用 Emulate 人體模擬系統發表的文章數已超過 100 篇，在同類產品中大幅領先。Emulate 相信，人類生物學和器官晶片技術的結合能夠點燃人類健康的新時代。

level Discovering new boundaries

進階生物科技股份有限公司

台北總公司 02-26959935　免付費專線 0800251302　傳真 02-26958373

www.level.com.tw

進階官網　FB粉絲團

emulate

IMPROVE

CLINICAL SUCCESS.

PATIENT SAFETY.

R&D PRODUCTIVITY.

HUMAN HEALTH.

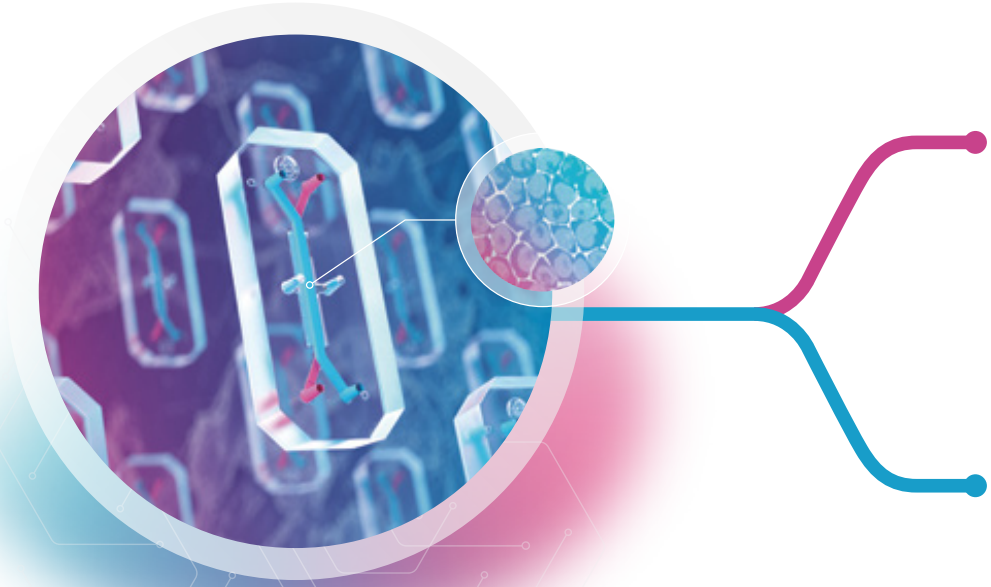

Emulate 器官晶片系統

The Human Emulation System® -- a complete Organ-on-a-Chip solution for next-generation in vitro models

7+充分驗證器官模型

肝臟晶片　腎臟晶片　結腸晶片　十二指腸晶片

肺泡晶片　肺氣道晶片　腦晶片　持續研發中

100+高影響力學術論文

- 細胞與基因治療
- 免疫治療
- 疫苗研究
- 腫瘤研究
- 毒性預測
- 表型鑒定
- .....

75+標準化指南390+專利/標準

100+用戶開發醫藥應用方向

ADME-Tox　腫瘤　神經科學　基因治療　CAR-T　血腦屏障　生殖

感染　微生物　炎症　藥物遞送　病毒　皮膚　.....

emulate

Emulate 的技術來源和沉澱

2010年，哈佛大學Wyss研究所創始系主任Donald E. Ingber教授團隊開發了世界上第一個成功的器官晶片：肺晶片。隨後Emulate成立，將該技術進行商業化推廣。

HARVARD UNIVERSITY

WYSS INSTITUTE for Biologically Inspired Engineering

Donald E. Ingber
哈佛大學生物工程教授

不斷拓展的客戶群-藥企、頂尖科研機構、政府監管部門

全球Top 20藥企均為Emulate用戶/合作夥伴

Roche · Genentech · Pfizer · FDA · HARVARD UNIVERSITY

gsk GlaxoSmithKline · GILEAD · Takeda · REGENERON SCIENCE TO MEDICINE

COVANCE · Johnson & Johnson · INSTITUT PASTEUR · Public Health England · Stanford University

關於Emulate

Emulate 致力於開發類比人體生理特徵的器官晶片技術及其創新應用，以全面瞭解疾病發生規律和幫助評估藥物的真實反應，改善人類健康。目前，Emulate 提供經過驗證的肝、腎、十二指腸、結腸、肺、腦等器官晶片解決方案的同時支援客戶定制化的研究需求，是全球市場佔有率領先的器官晶片系統。已經被全球排名前 20 的藥企全部合作引入，採用 Emulate 器官晶片平臺發表的文章數已超過100篇，在同類產品中大幅領先。 Emulate 相信，人類生物學和器官晶片技術的結合能夠點燃人類健康的新時代。Emulate 總部位於美國波士頓，亞太區總部位於中國上海。

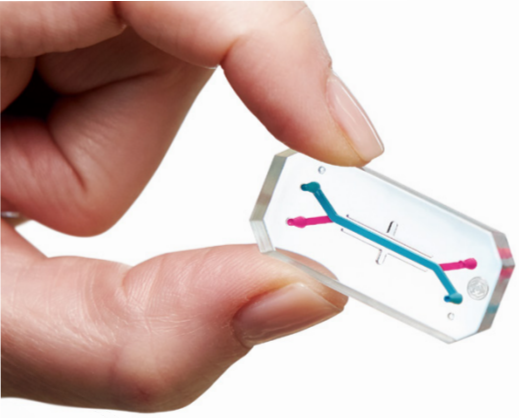

儀器系統

晶片耗材

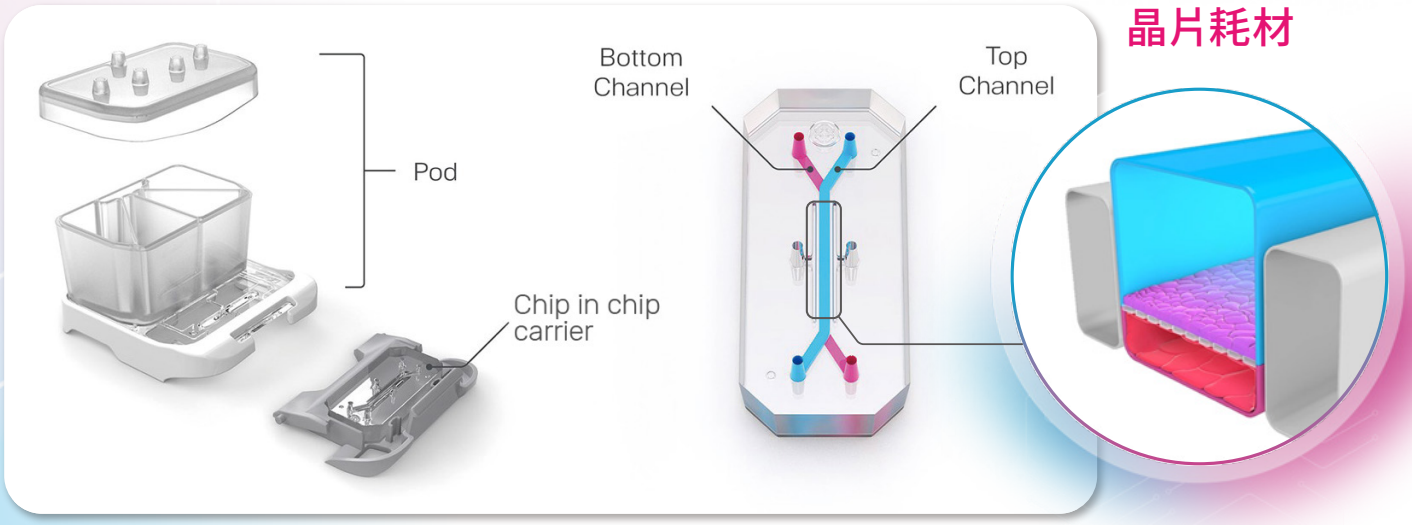

生物試劑

Bio-Kits: 充分驗證試劑套裝

組分: 晶片耗材、充分驗證的細胞
教程: 充分驗證的器官模型構建教程和指南
支持: 經驗豐富的學術/技術支援，專業的科學家團隊

Basic Research Kit: 用戶自研套裝

組分: 晶片耗材
細胞: 用戶自有，原代細胞, iPSC, 類器官球, 細胞系等全相容
教程: 基礎器官晶片構建教程，支援器官特異性參數調整和優化
支持: 經驗豐富的學術/技術支援，專業的科學家團隊